Progress in physics and control of the resistive wall mode in advanced tokamaks[a)]

Yueqiang Liu,[1,b)] I. T. Chapman,[1] M. S. Chu,[2] H. Reimerdes,[3] F. Villone,[4] R. Albanese,[5] G. Ambrosino,[4] A. M. Garofalo,[2] C. G. Gimblett,[1] R. J. Hastie,[1] T. C. Hender,[1] G. L. Jackson,[2] R. J. La Haye,[2] M. Okabayashi,[6] A. Pironti,[4] A. Portone,[7] G. Rubinacci,[5] and E. J. Strait[2]

[1]*Euratom/UKAEA Fusion Association, Culham Science Centre, Abingdon OX14 3DB, United Kingdom*
[2]*General Atomics, San Diego, California 92186, USA*
[3]*Columbia University, New York, New York 10027, USA*
[4]*ENEA/CREATE, DAEIMI, Universita di Cassino, Via di Biasio 43, I-03043 Cassino (FR), Italy*
[5]*ENEA/CREATE, Universita Federico II di Napoli, Via Claudio 21, I-80125 Napoli, Italy*
[6]*Princeton Plasma Physics Laboratory, Princeton, New Jersey 08543, USA*
[7]*Fusion For Energy, C/Josep Pla 2, B3, 08019 Barcelona, Spain*

(Received 4 December 2008; accepted 2 April 2009; published online 29 April 2009)

Self-consistent computations are carried out to study the stability of the resistive wall mode (RWM) in DIII-D [J. L. Luxon, Nucl. Fusion **42**, 614 (2002)] plasmas with slow plasma rotation, using the hybrid kinetic-magnetohydrodynamic code MARS-K [Y. Q. Liu *et al.*, Phys. Plasmas **15**, 112503 (2008)]. Based on kinetic resonances between the mode and the thermal particle toroidal precession drifts, the self-consistent modeling predicts less stabilization of the mode compared to perturbative approaches, and with the DIII-D experiments. A simple analytic model is proposed to explain the MARS-K results, which also gives a qualitative interpretation of the recent experimental results observed in JT-60U [S. Takeji *et al.*, Nucl. Fusion **42**, 5 (2002)]. Our present analysis does *not* include the kinetic contribution from hot ions, which may give additional damping on the mode. The effect of particle collision is *not* included either. Using the CARMA code [R. Albanese *et al.*, IEEE Trans. Magn. **44**, 1654 (2008)], a stability and control analysis is performed for the RWM in ITER [R. Aymar *et al.*, Plasma Phys. Controlled Fusion **44**, 519 (2002)] steady state advanced plasmas, taking into account the influence of three-dimensional conducting structures.
[DOI: 10.1063/1.3123388]

I. INTRODUCTION

It has long been realized that the resistive wall mode (RWM) instability, being the ultimate pressure limiting factor for steady state advanced tokamaks,[1] needs to be understood and controlled.[2] This mode is traditionally studied in the magnetohydrodynamic (MHD) framework as a global external kink instability, whose growth rate is greatly suppressed (by several orders of magnitude) by the presence of external conducting structures (e.g., vacuum vessels) surrounding the plasma, but the mode does grow on the resistive time scale of the vessel, as the vessel eddy currents decay.

The rotational damping has been a major piece of physics investigated in the MHD theory for the RWM. According to ideal MHD, the mode resonance with stable waves such as Alfvén waves[3,4] or sound waves,[5,6] occurring at sufficiently fast plasma toroidal rotation (at least a few percent of the Alfvén speed), damps free energy of the mode, and can lead to its suppression. Nonideal MHD effects, such as resistive layer damping[7,8] or viscous boundary layer damping[9] can also lead to mode stabilization.

However, recent experimental results on several tokamak machines including DIII-D (Refs. 10 and 11) and JT-60U (Ref. 12) suggest that the RWM can be much more stable than the conventional MHD theory predicts. It has been suggested that certain strong damping physics, coming from kinetic effects such as the mode resonance with various plasma particle drift motions, can explain the experimental observations. At relatively fast plasma rotation, the additional kinetic damping may come from the mode resonance with the transit or bounce motion of thermal ions from the bulk plasma.[13,14] At slow plasma rotation (below the ion diamagnetic flow speed), a strong damping is predicted coming from the mode resonance with toroidal magnetic precession drifts of trapped thermal ions and electrons.[15]

The first part of this paper (Sec. II) presents a systematic investigation of the kinetic effects on the stability of the RWM. In particular, we model some experimental high performance plasmas from DIII-D, where the plasma fluid rotation is kept low by using balanced neutral beam injection. These plasma conditions simulate ITER (Ref. 16) steady state advanced scenarios.

The modeling is based on a recently developed hybrid kinetic-MHD code MARS-K.[17] This code solves a self-consistent nonlinear eigenvalue problem which couples single fluid, linear MHD equations with perturbed kinetic pressure tensors, analytically derived by solving the linearized drift kinetic equation.[18,19] The kinetic pressure tensor terms are represented in the form of kinetic integrals over the particle velocity phase space (eventually over the particle

[a)]Paper BI2 3, Bull. Am. Phys. Soc. **53**, 22 (2008).
[b)]Invited speaker. Electronic mail: yueqiang.liu@ukaea.org.uk.

kinetic energy and pitch angle), and a simplification is sought by assuming a vanishing banana width for the particle orbit.

The detailed formulation is presented in Ref. 17. We just point out here that the self-consistency of the formulation is reflected in three aspects. (1) The mode eigenfunction, which enters into the kinetic pressure tensors, is self-consistently modified by the kinetic effects. Hence it may not necessarily be the fluid eigenfunction. (2) The mode eigenvalue, as a complex mode frequency, enters into the kinetic integrals for kinetic pressure tensors in a nonlinear fashion. This results in a nonlinear eigenvalue problem that we have to solve, in order to determine the stability of the kinetic RWM. A simple analytic model, proposed in Sec. III, illustrates this nonlinear coupling. (3) The MHD types of damping, such as the shear Alfvén and the sound wave damping, are automatically maintained in the self-consistent kinetic calculations.

On the other hand, the perturbative approach, followed by the MISK code[15] and the HAGIS code,[20,21] as well as by the MARS-K code as one of its options, uses the fluid eigenfunction (marginally stable ideal kink or fluid RWM) to evaluate the kinetic integrals. The complex mode frequency in the kinetic integrals is normally assumed to be a constant (fluid RWM eigenfrequency or simply zero). The shear Alfvén damping is normally added *a posteriori*.

The MARS-K code has been successfully benchmarked with the HAGIS code.[17] The latter is a drift kinetic particle-orbit following code, which takes into account the true particle guiding center orbit (including the effect of finite banana width for trapped particles) in computing the drift kinetic resonances. The agreement between the two codes validates the approximation of zero banana width made in the MARS-K formulation (as well as in the MISK formulation). MARS-K has also been used to study the RWM stability in ITER.[22] Here, we report the modeling results for DIII-D plasmas, following both perturbative and self-consistent approaches in MARS-K.

The second part of the paper (Sec. IV) presents our recent study of the RWM for ITER steady state plasmas, where the emphasis is on investigating the influence of the realistic three-dimensional (3D) geometry of ITER walls on the mode stability and control. Here we use the CARMA code,[23,24] which couples self-consistently the MHD code MARS-F (Ref. 25) and the 3D eddy current code CARIDDI.[26] The coupling procedure between two codes has been rigorously proven in analytical theory.[27,28] The CARMA code has been benchmarked against other similar 3D codes, such as VALEN (Ref. 29) and STARWALL,[30] as well as against the experimental results in RFX (Ref. 31) for the passive growth rates of the RWM with 3D walls.

A unique feature of CARMA is that the code has the possibility of using the state-of-the-art fast method, based on the singular value decomposition technique,[32] for solving large scale eddy current problems. This technique helps to reduce the computational cost of inverting a full matrix from $O(N^3)$, with conventional methods, to $O(N \log N)$, where N is the number of degrees of freedom (DoF). As a result, it is possible to solve a large problem, with the number of DoF exceeding 10^5 on a present desktop-type computer with reasonable performance. This allows CARMA to model volumetric conducting elements such as the blanket modules in ITER, without using a thin-shell approximation.

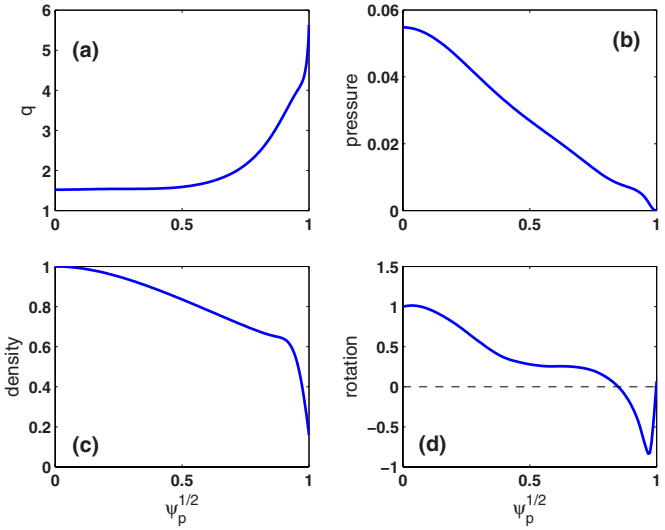

FIG. 1. (Color online) Equilibrium profiles, from the DIII-D discharge 125 701 at 2.5 s, used in the modeling, for (a) safety factor q, (b) plasma pressure normalized by B_0^2/μ_0, (c) plasma density normalized by the central value, and (d) $E\times B$ drift frequency profile normalized by the central amplitude. ψ_p is the normalized poloidal magnetic flux.

II. MODELING RESULTS FOR DIII-D PLASMAS

In the modeling results shown below for the DIII-D plasmas, we include only precessional drift resonances of thermal particles for the drift kinetic calculations since our primary objective is to investigate the kinetic effects on the RWM stability with slow plasma rotation, as in the DIII-D experiments with balanced beam injection. A slow plasma rotation is also expected in the ITER steady state plasmas.[14] In fact, a similar study for the ITER plasmas reveals that the kinetic contribution from bounce resonances of thermal ions is relatively small even at a reasonably fast rotation speed.[22]

Another important piece of physics that is missing in the following study is the kinetic effects from hot ions induced by the neutral beam injection. This may have a significant consequence on the conclusion, when the modeling results are compared to the experiments. The effect of particle collision, though already implemented in the MARS-K code, is not included in the present computations.

A. DIII-D equilibrium used in computations

Figure 1 shows the equilibrium profiles, reconstructed from the DIII-D discharge 125 701 at 2.5 s,[33] that we use to study the kinetic effects on the RWM using MARS-K. The plasma major radius is $R_0=1.7$ m. The toroidal magnetic field at the magnetic axis is $B_0=1.7$ T. The total plasma current is $I_p=1.14$ MA. In order to find the beta limits, we scale the amplitude of the plasma equilibrium pressure without modifying the pressure profile shown in Fig. 1(b), as well as keeping the total plasma current unchanged. (The surface averaged plasma current density profile is also fixed.) The computed no-wall limit for the $n=1$ ideal kink instability is

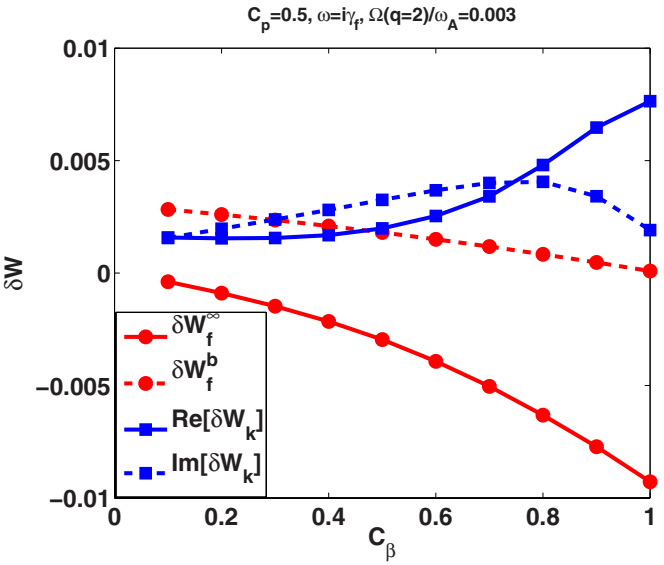

FIG. 2. (Color online) Computed perturbed fluid and drift kinetic potential energies for a case with $\omega_E(q=2)/\omega_A=0.3\%$, $C_P=0.5$, and $\omega=i\gamma_f$. The eigenfunction of the fluid RWM without flow is used for the kinetic energy evaluation in the perturbative approach.

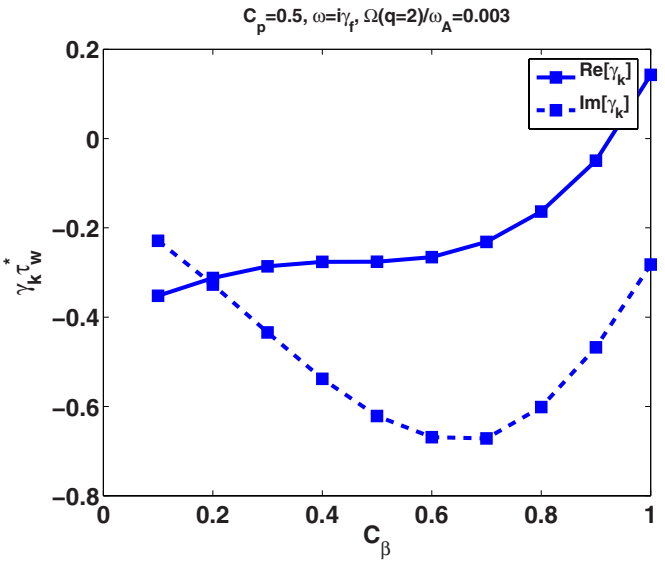

FIG. 3. (Color online) Computed eigenvalue of the kinetic RWM, following the perturbative approach, for the same case, as shown in Fig. 2.

$\beta_N^{\text{no-wall}}=1.93$, and the ideal-wall limit is $\beta_N^{\text{ideal-wall}}=3.11$. $\beta_N\equiv\beta(\%)a(\text{m})B_0(\text{T})/I_p(\text{MA})$ is the normalized beta, with β being the ratio of the plasma gasokinetic pressure to the magnetic pressure and a the plasma minor radius. A thin-wall approximation is used in MARS-K for the nonconformal, DIII-D vacuum-vessel shell. Following convention, a pressure scaling factor is defined as $C_\beta=(\beta_N-\beta_N^{\text{no-wall}})/(\beta_N^{\text{ideal-wall}}-\beta_N^{\text{no-wall}})$. The experimental plasma pressure corresponds to C_β of about 0.55.

The $E\times B$ drift frequency (ω_E) profile shown in Fig. 1(d) is obtained at $t=2.5$ s when the RWM is marginally stable in experiments. The critical ω_E frequency is about 0.3% of the Alfvén frequency $\omega_A\equiv B_0/(R_0\sqrt{\mu_0\rho_0})$ at the $q=2$ radial position,[10] where ρ_0 is the plasma central density. We point out that some of the recent DIII-D experiments seem to suggest an even lower critical rotation frequency for the RWM.[34] In the study, we also scale the $E\times B$ rotation amplitude without changing the profile shown in Fig. 1(d).

B. Computation results using perturbative approach

In the perturbative approach, the stability of the RWM is determined by the following extended RWM dispersion relation,[35,36] derived from the kinetic MHD energy principle:

$$\gamma\tau_w^*\simeq-\frac{\delta W_\infty+\delta W_k}{\delta W_b+\delta W_k},\qquad(1)$$

where τ_w^* is the typical wall eddy current decay time. δW_∞ and δW_b are the fluid potential energies without and with a conducting wall, respectively. The fluid energy includes both the plasma and the vacuum contributions. δW_k is the perturbed drift kinetic energy. In all the computed results shown here with perturbative approach, δW_k is computed using the eigenfunction of the fluid RWM.

Figure 2 shows one example of the computed perturbed potential energies (both fluid and drift kinetic portions) versus the parameter C_β, for a case where we assume a rotation frequency $\omega_E(q=2)/\omega_A=0.3\%$ and an equal equilibrium temperature for thermal ions and electrons: $C_P\equiv T_i/(T_i+T_e)=0.5$. In this perturbative analysis, the complex mode frequency that enters into the drift kinetic integrals is assumed to be the fluid RWM frequency $\omega=i\gamma_f$. The fluid potential energies, computed for an ideal kink mode without wall and with an ideally conducting wall, are both real. The drift kinetic energy, computed using eigenfunctions of the fluid RWM at corresponding C_β, has both real (inertial) and imaginary (damping) parts. The real part increases monotonically with the plasma pressure for this case. We notice that the magnitude of the drift kinetic energy perturbation is comparable to the fluid energy perturbation, indicating a strong effect on the stability of the RWM by kinetic terms, following the perturbative approach.

Indeed, Fig. 3 shows the eigenvalue of the kinetic RWM, calculated using the dispersion relation (1), for the same case as in Fig. 2. The negative real part of the eigenvalue, for $C_\beta\lesssim0.9$, shows that the mode is completely stabilized by the drift kinetic effects (with the assumptions used in this perturbative approach). The mode is still unstable (partial stabilization) for $C_\beta\gtrsim0.9$.

Figure 4, for the same equilibrium parameters as Fig. 3, shows a two-dimensional (2D) scan of growth rate of the kinetic RWM, over the parameter space in C_β and ω_E, two of the most important parameters determining the stability of a fluid RWM. The black dots in Fig. 4(a) indicate the region where the RWM is completely stabilized by the kinetic effects. The perturbative approach predicts a strong stabilization of the RWM for DIII-D plasmas, over a wide range of the parameter space. This seems to coincide with the present interpretation of the experimental results on DIII-D.

The real mode frequency, induced purely by the kinetic effects and shown in Fig. 4(b), tends to vanish at both low and high rotation frequencies, and reaches its maximum near

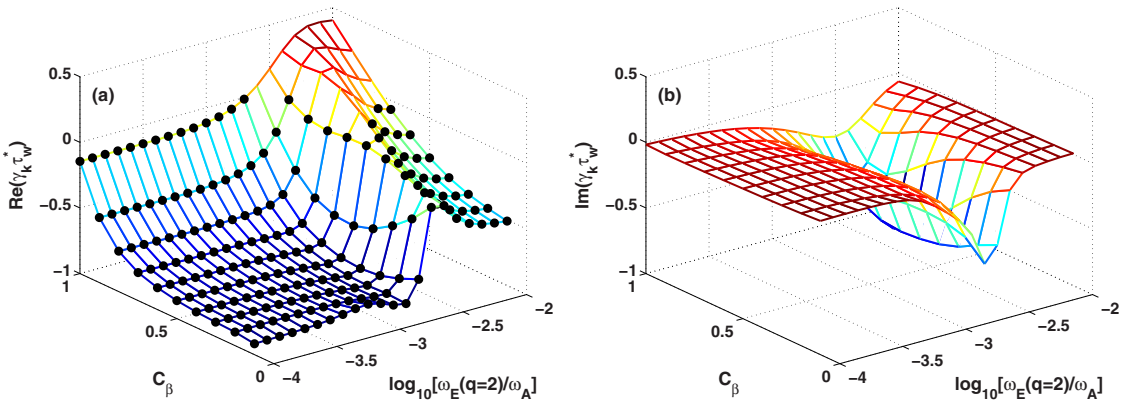

FIG. 4. (Color online) 2D plots of the (a) real and (b) imaginary parts of the kinetic RWM eigenvalue following the perturbative approach, for the case with $C_P=0.5$, $\omega=i\gamma_f$. The black dots indicate a stable RWM.

$\omega_E=10^{-3}\omega_A$, which belongs to the typical range of the thermal particle precession drift frequencies for DIII-D plasmas.

The strong kinetic stabilization of the mode is relatively insensitive to assumptions made in the kinetic energy evaluations. Figures 5 compares the contour plots of the real part of the kinetic RWM for three cases: (a) the reference case with $C_P=0.5$, $\omega=i\gamma_f$, as shown in Figs. 4(a), (b) a case with the equilibrium ion temperature larger than the electron temperature $C_P=0.6$ (as in the experiment $T_i>T_e$), $\omega=i\gamma_f$, and (c) a case where the drift kinetic integrals are evaluated neglecting the fluid RWM mode frequency $C_P=0.5$, $\omega=0$. The solid lines in all figures indicate the stability boundary in the parameter space (C_β,ω_E). Following the perturbative approach, a larger fractional ion kinetic contribution in this case leads to a stronger mode stabilization. A similar observation is made in an analytic large-aspect-ratio calculation.[37] Neglect of the fluid RWM eigenfrequency in the kinetic integrals results in a sharper transition between the stable and unstable regions.

C. Computation results using self-consistent approach

The stability of the kinetic RWM in DIII-D is investigated for various choices of plasma parameters, following the self-consistent approach in MARS-K. Figures 6(a) and 6(b) show two examples of the computed eigenvalue of the kinetic RWM versus ω_E, for cases with $C_\beta=0.5$, and $C_P=0.5$ and 0.6, respectively. For a comparison, plotted are also the eigenvalues of the fluid RWM, subject to the MHD type of continuum damping (the Alfvén and sound wave damping) in a rotating plasma.

Two unstable branches of the solutions are observed in the self-consistent kinetic computations for both $C_P=0.5$ and 0.6. For the choice of parameter $C_P=0.5$, there is a narrow window between these two unstable branches, near $\Omega(q=2)/\omega_A\simeq 1.5\times 10^{-3}$, where the RWM is almost completely stabilized by including the magnetic drift resonance damping of trapped thermal particles. This stable window disappears for the case with $C_P=0.6$. In both cases, however, the mode remains unstable at ω_E slower than $\Omega(q=2)/\omega_A\simeq 1.5\times 10^{-3}$. This unstable branch is not obtained following the perturbative approach. Also note that for this branch, the mode frequency remains finite even when the $E\times B$ rotation frequency approaches zero. This mode frequency is not sensitive to the equilibrium ion-electron temperature ratio.

At higher plasma pressures, the self-consistent computations also find three unstable branches. Figures 7(a) and 7(b) compare the reference case at intermediate pressure $C_\beta=0.5$ with a high pressure case $C_\beta=0.8$. Three unstable branches, with distinct real mode frequencies, are seen in Fig. 7(b).

Figure 8 show 2D plots of the self-consistently computed eigenvalue of the kinetic RWM in the parameter space

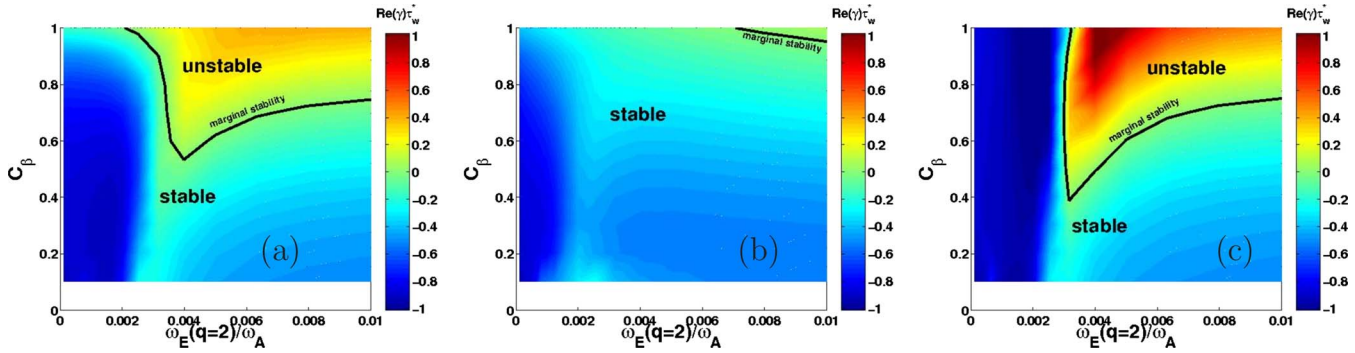

FIG. 5. (Color online) Comparison of the real part of the kinetic RWM eigenvalues, computed using the perturbative approach. Three cases are compared to (a) $C_P=0.5$, $\omega=i\gamma_f$ [the same as in Fig. 4(a)], (b) $C_P=0.6$, $\omega=i\gamma_f$, and (c) $C_P=0.5$, $\omega=0$.

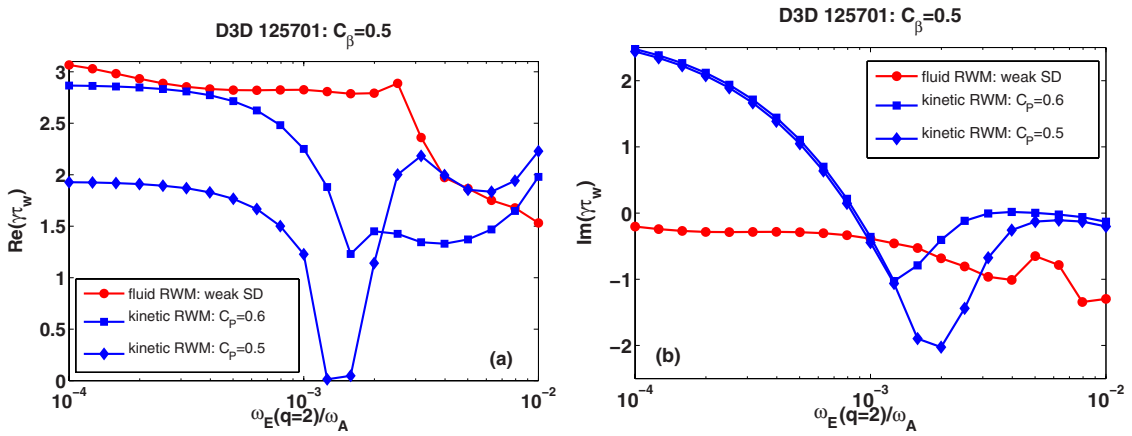

FIG. 6. (Color online) The (a) real and (b) imaginary parts of the growth rate of the RWM vs ω_E, computed using the self-consistent approach for the DIII-D plasma, with C_β=0.5.

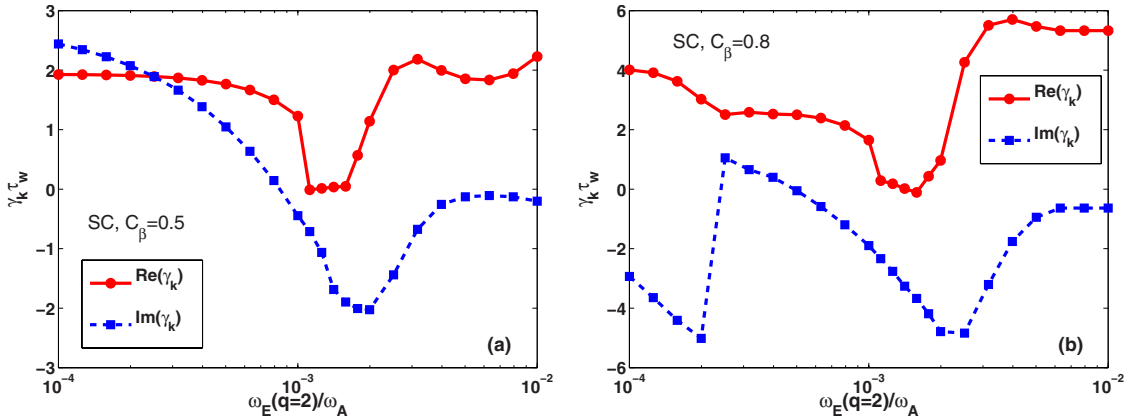

FIG. 7. (Color online) The eigenvalue of the kinetic RWM vs ω_E for (a) C_β=0.5, C_P=0.5, and (b) C_β=0.8, C_P=0.5, following the self-consistent (SC) calculations.

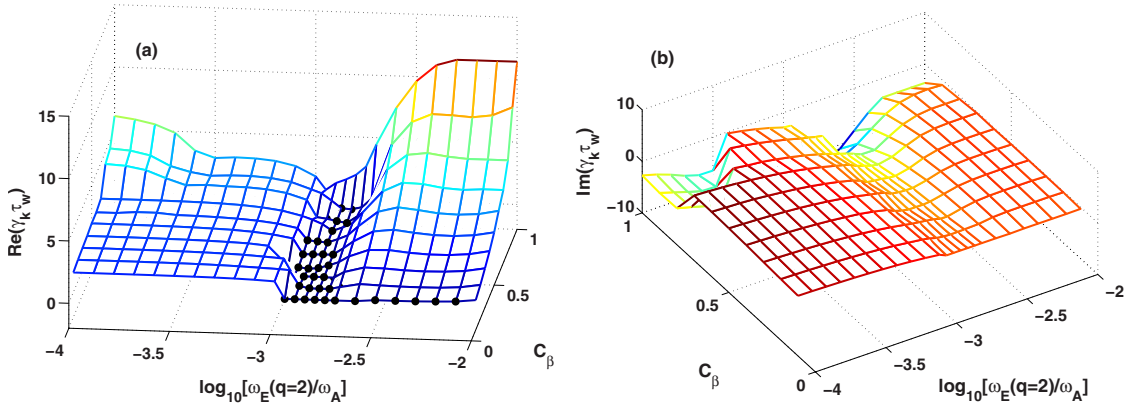

FIG. 8. (Color online) 2D plots of the (a) real and (b) imaginary parts of the kinetic RWM eigenvalue following the self-consistent approach, for the case with C_P=0.5. The black dots indicate a stable RWM.

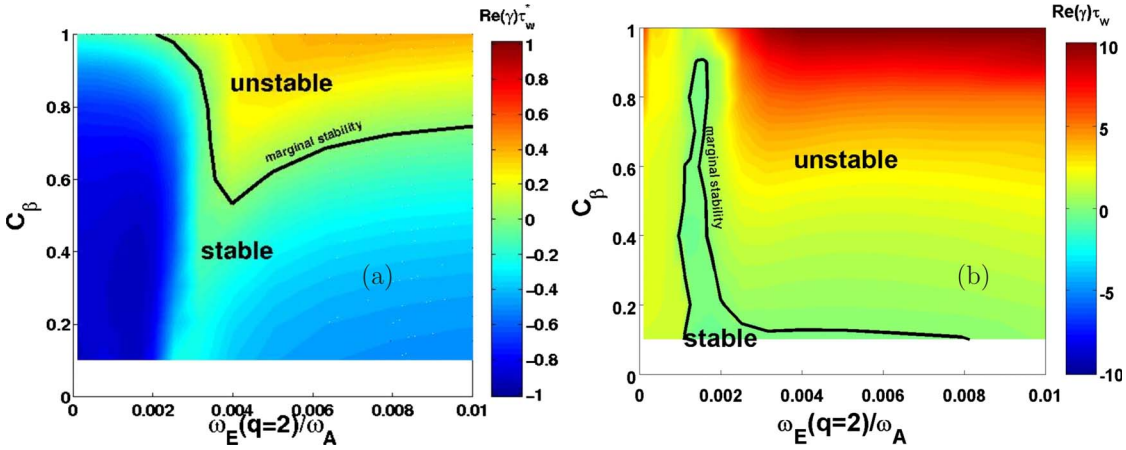

FIG. 9. (Color online) Comparison of the real part of the kinetic RWM eigenvalue between (a) perturbative [the same as Fig. 5(a)] and (b) self-consistent approaches. A case with $C_P=0.5$ is considered.

(C_β, ω_E), for the case with an equal equilibrium ion-electron temperature. Only a narrow valley of stability is obtained, indicated by black dots. The stable region is not sensitive to the plasma pressure C_β.

D. Discussion

The difference between the perturbative and the self-consistent results is clearly shown by comparing the contour plots in Figs. 9(a) and 9(b). The wide stable region, predicted by the perturbative approach, is significantly shrunken following the self-consistent approach due to the onset of additional unstable branches of the solutions. It is interesting to mention again that the experimental plasma, where the RWM is marginally stable, has $C_\beta \simeq 0.55$ and $\omega_E(q=2)/\omega_A=0.003$. For these parameters, the self-consistent approach predicts an unstable RWM. The difference between the self-consistent computation results and the experiments indicates that probably some additional damping physics, which is not considered in this study, needs to be taken into account, in order to fully explain the experimental data in DIII-D.

Besides the difference between the computation results and the experimental observations, it is also important to understand what causes the significant difference between the perturbative and the self-consistent results. There are two major factors that can potentially contribute to this. One is the possibility of the kinetic modification of the RWM eigenfunction in the self-consistent approach. This indeed occurs for certain analytical toroidal equilibria.[17] The other possibility comes from the nonlinear eigenvalue formulation, as a result of the nonlinear coupling of the mode complex frequency ω to the drift kinetic integrals via the resonant conditions. We investigate both possibilities.

Figure 10 compares eigenfunctions for three modes: the no-wall ideal kink mode, the fluid RWM used in the perturbative approach, and the kinetic RWM from the self-consistent approach. The prominent difference in the eigenfunctions between the no-wall ideal kink and the fluid RWM, near rational surfaces, is understandable, since the width of the inertial layer near rational surfaces is proportional to the mode growth rate, which is different by orders of magnitude between the kink and the RWM. There is, however, no significant difference between the eigenfunctions for the fluid RWM and the self-consistent kinetic RWM. This observation, though not general, does occur also for the toroidal, pressure driven RWM in ITER steady state plasmas.[22]

Since the first possibility does not seem to explain the difference between the perturbative and the self-consistent results, we turn to the second possibility, i.e., the nonlinear eigenvalue formulation via the kinetic integrals. We devise a

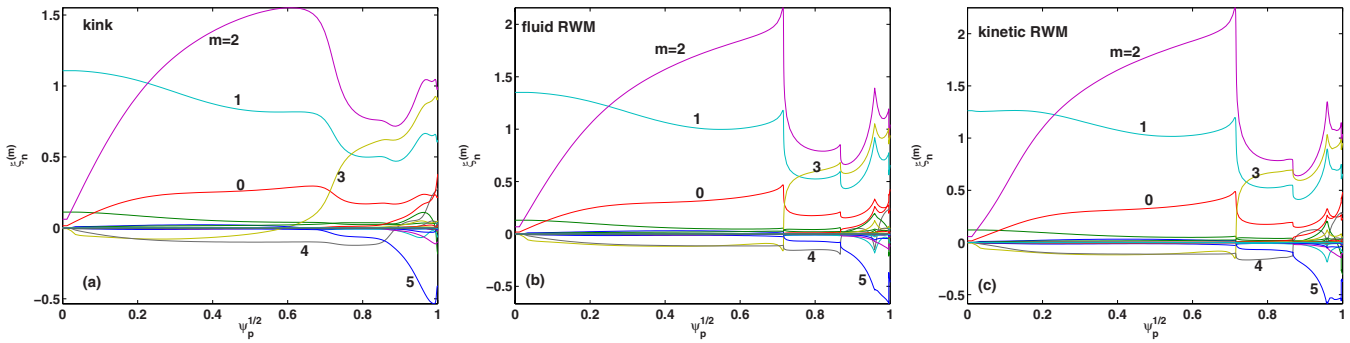

FIG. 10. (Color online) Comparison of the poloidal Fourier harmonics of normal displacement vs the plasma minor radius, for (a) no-wall ideal kink mode, (b) fluid RWM, and (c) kinetic RWM from the self-consistent calculations. The other parameters, where applicable, are $C_\beta=0.5$, $C_P=0.5$, and $\omega_E(q=2)/\omega_A=0.003$. An equal-arc coordinate system is used in the MARS-K computations. ψ_p is the normalized poloidal magnetic flux.

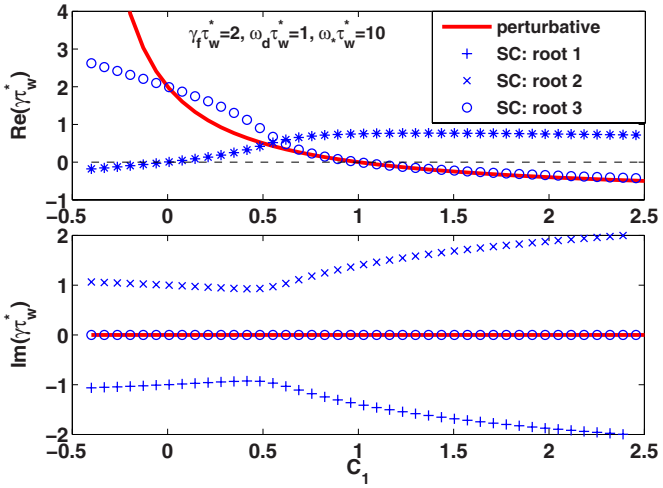

FIG. 11. (Color online) Growth/damping rate of the kinetic RWM vs $C_1 \equiv C(0)$, following the dispersion relation (3). A typical set of parameters is chosen: $\hat{\gamma}_f=2$, $\hat{\omega}_d=1$, and $\hat{\omega}_*=10$. The growth rate of the mode from a perturbed approach [let $C=C_1$ in Eq. (3)] is also plotted as solid lines. Note that roots 1 and 2 are complex conjugates, hence symbols "+" and "×" in the upper panel overlap to form "*."

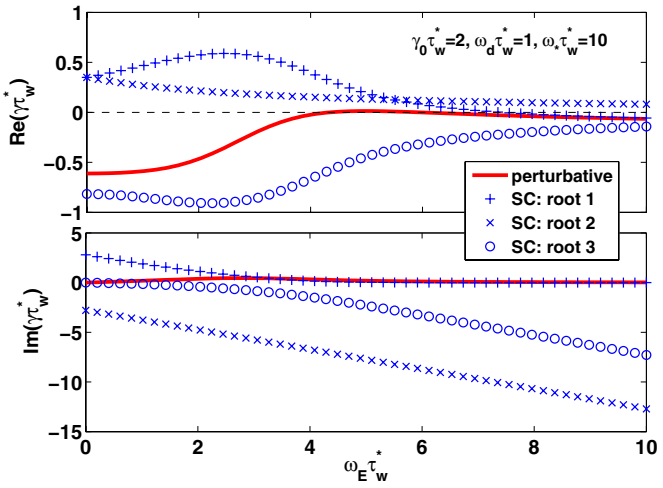

FIG. 12. (Color online) Eigenvalues of the kinetic RWM vs ω_E: (top) real and (bottom) imaginary part of the eigenvalue. Perturbative approach (solid line) assumes $\omega=i\gamma_f$. Nonlinear eigenvalue formulation via the kinetic integrals results in three roots (markers). Other parameters are the same as in Fig. 11, except for $C_1=12$.

simple analytic model to demonstrate this nonlinear effect. An initial version of this model is reported in Ref. 17.

III. A SIMPLE ANALYTIC MODEL

The key factor in the perturbed kinetic energy δW_k is the mode particle resonance operator.[28] By keeping only this factor in δW_k and dropping the kinetic integrals over the particle energy and pitch angle, we have

$$\delta W_k \sim c\left[\frac{\omega_{*i}+\omega_E-i\gamma}{\omega_{di}+\omega_E-i\gamma}+\frac{\omega_{*e}+\omega_E-i\gamma}{\omega_{de}+\omega_E-i\gamma}\right], \tag{2}$$

where ω_{*i} and ω_{*e} are the typical diamagnetic frequencies for thermal ions and electrons, respectively, and ω_{di} and ω_{de} can be viewed as "lumped" precession drift frequencies for ions and electrons, respectively, over the particle kinetic energy and pitch angle. The coefficient c "lumps" all the other factors participating into the kinetic energy potential, including the mode eigenfunction, which we assume now is not modified by the kinetic effects. Note that for simplicity, we consider only the magnetic precessional drift resonances in this model.

As a further simplification, we consider cases with $\omega_{*i}=-\omega_{*e}=\omega_*$ and $\omega_{di}=-\omega_{de}=\omega_d$. This roughly corresponds to $C_P=0.5$.

Combining Eq. (2) with Eq. (1), we obtain a nonlinear dispersion relation for the eigenvalue of the kinetic RWM,

$$\hat{\gamma}=\frac{1-C(\hat{\gamma})}{\hat{\gamma}_f^{-1}+C(\hat{\gamma})}, \quad C(\hat{\gamma})=2c\frac{\hat{\omega}_*\hat{\omega}_d+(\hat{\gamma}+i\omega_E)^2}{\hat{\omega}_d^2+(\hat{\gamma}+i\omega_E)^2}, \tag{3}$$

where all the frequencies and the mode growth rate are normalized by the choice of the wall time τ_w^* as defined in Ref. 36, and $\hat{\gamma}_f$ represents the normalized growth rate of the fluid RWM.

The dispersion relation (3) results in a cubic equation for the mode growth rate $\hat{\gamma}$. It is interesting first to study the case with vanishing rotation $\hat{\omega}_E=0$. Figure 11 shows the three roots for the self-consistent formulation, and compares with the single root from the perturbative approach, where we have denoted $C_1=C(0)$ in Eq. (3). Three ranges of C_1 can be identified. For $C_1<0$, the perturbative approach predicts destabilization of the RWM compared to the fluid theory. The self-consistent approach predicts one unstable branch, with the growth rate between the fluid and the perturbative values, and two stable branches (complex conjugate) with finite frequency. For $C_1>1$, the perturbative approach predicts complete stabilization, while the self-consistent approach gives one stable branch close to the perturbative result, and two unstable branches with finite mode frequency. The latter corresponds to what we observe in Fig. 6, at the very slow rotation limit. For $0<C_1<1$, we observe a smooth transition between the two regimes described above. In particular, the self-consistent calculation predicts less stabilization than the perturbative approach, as already pointed out in Ref. 37.

Now we scan the three roots from the nonlinear dispersion relation over the rotation frequency $\hat{\omega}_E$, for a case where the perturbative approach predicts deep stabilization of the mode ($C_1=12$). To avoid a singularity problem, we will assume that the eigenvalue of the fluid RWM $\hat{\omega}=i\hat{\gamma}_f$ is used in the kinetic resonance operator for the perturbative approach. This is the assumption that we normally use in the toroidal perturbative computations. Figure 12 compares the single root from the perturbative approach with the three roots from the self-consistent approach. Again two unstable branches are obtained, which are not complex conjugate anymore due to the finite rotation frequency. These two unstable branches are qualitatively similar to that computed by MARS-K for DIII-D plasmas, as shown in Fig. 7(a), thus explaining the numerical results obtained with the self-consistent approach. By varying the value of parameter C_1 (between 0 and 1) in the analytic model, it is also possible to obtain three unstable roots, confirming the DIII-D computation results, as shown in Fig. 7(b).

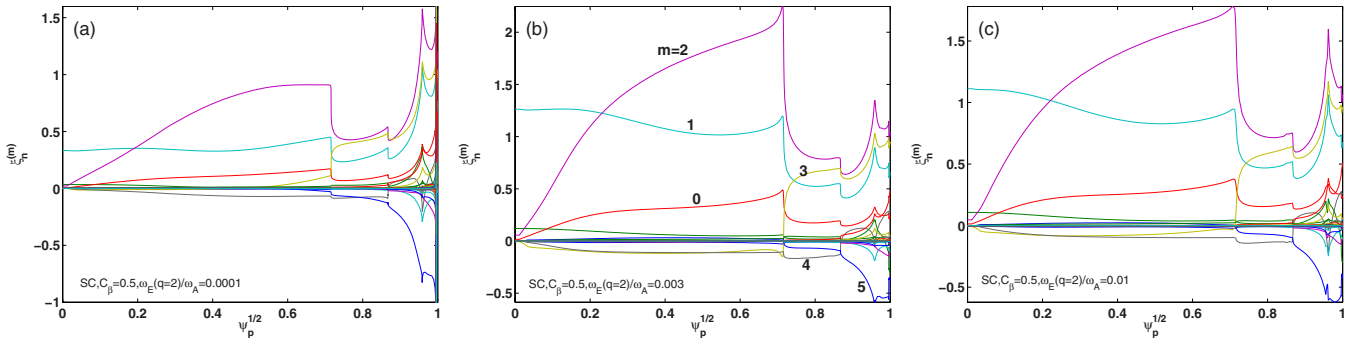

FIG. 13. (Color online) Comparison of the poloidal Fourier harmonics of normal displacement vs the plasma minor radius, obtained from the self-consistent computations for a DIII-D plasma with C_β=0.5, C_P=0.5, and $\omega_E(q=2)/\omega_A$ equal to (a) 0.01%, (b) 0.3%, and (c) 1%.

A close look at these two unstable roots from Fig. 12 reveals the following features. For one of the unstable roots, labeled by "x," the mode remains unstable at fast enough rotation and grows on the time scale longer than the wall time. The mode frequency largely follows (slightly exceeds) the rotation frequency. These two features resemble that of the so-called slowing growing RWM (or the RWM precursor) observed in the recent JT-60U experiments.[38] As the plasma rotation slows down, the other unstable root (labeled by "+") appears and becomes dominant. This mode eventually grows at the wall time. The mode frequency is small. These two features are similar to that observed for the ordinary RWM in JT-60U. We note that, according to the perturbative approach, the fluid RWM is fully stabilized by the kinetic effects in this case (the solid lines). In the experiments, a bursting mode (EWM) is also observed at fast plasma rotation, which is identified as an energetic particle driven mode. This mode grows at the wall time scale, with a frequency sweeping that initially does not match the plasma rotation frequency. This mode is not predicted by our self-consistent model. Instead, the model gives a stable root (labeled by "o"), with the mode frequency largely following, but smaller than, the rotation frequency.

The JT-60U experiments report that all the unstable modes (EWM, RWM precursor, and the conventional RWM) have a kink-ballooning structure.[38] This is also confirmed by the MARS-K self-consistent calculations. Shown in Fig. 13 are the eigenmode structures of the kinetic RWM, computed following the self-consistent approach for the DIII-D case shown in Fig. 7(a). We find that all the three eigenfunctions from two unstable branches (when $\omega_E(q=2) \lesssim 1.5\times10^{-3}\omega_A$ and when $\omega_E(q=2) \gtrsim 1.5\times10^{-3}\omega_A$), although not identical to each other, do have the RWM eigenstructure, which is kink-ballooning-like.

We point out that the model proposed here is a lumped, qualitative model, which implies that (i) the parameter space covered by this model may not necessarily reflect the realistic parameter space; (ii) a more comprehensive model, for instance by taking into account more appropriately the kinetic integration in the particle velocity space, may not necessarily result in a three-root solution.

IV. RWM MODELING FOR ITER WITH 3D CONDUCTORS

As mentioned in the Introduction, we use the CARMA code to study the RWM in ITER, where 3D features of external conducting structures (walls, coils, etc.) may play a significant role in the mode stability and control. No plasma rotation and no kinetic effects are included in this investigation, although it will certainly be very useful to include these effects in future studies. We use the same ITER equilibria, as in Ref. 14. This section does not aim to cover the full aspects of CARMA modeling results for ITER, but rather focuses on representative examples.

A. 3D geometry of ITER walls

Figure 14 shows one example of ITER wall geometry used in the CARMA computation. Several 3D features are included such as the outer triangular support (OTS), the wall holes, and the tubular extensions.

B. Passive growth rates of the RWM

Table I summarizes the computed passive growth rates of the RWM in ITER steady state plasmas, under various assumptions for the wall geometry. The growth rates, computed by the MARS-F code[25] with complete, axisymmetric, double thin shells, are listed as reference values. CARMA computes similar growth rates by assuming a 2D wall geometry (but with a 3D meshing). However, by assuming a double wall with simple holes, CARMA predicts much larger growth rates for the RWM, as shown by the fifth column in Table I. The growth rate of the RWM is two to three times larger than that with a 2D complete double wall. On the other hand, simple holes are not a realistic description of the ITER wall geometry because of the presence of the tubular extensions, which effectively allow a better flow of the eddy currents in the conductors, hence a better stabilization of the mode. The CARMA computations for this case (6th column) predict growth rates which are much less than that with the simple hole approximation, and in fact more closer to that predicted with 2D complete walls. Therefore, the simple hole assumption that has been used previously for the RWM stability computations in ITER leads to a too pessimistic pre-

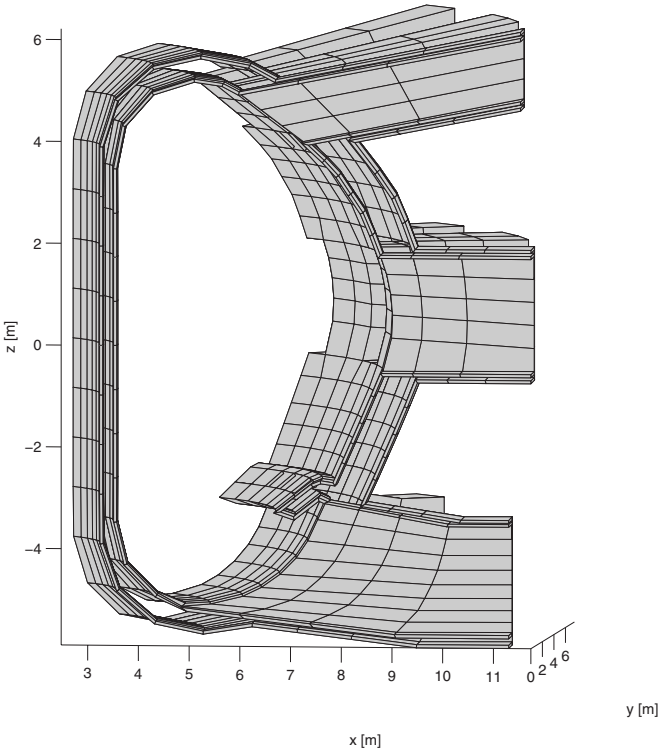

FIG. 14. Geometry of 3D ITER walls used in the RWM modeling by CARMA. Only one section along the toroidal angle is shown. Included in the geometry are the OTS with bypass, wall holes, and tubular extensions.

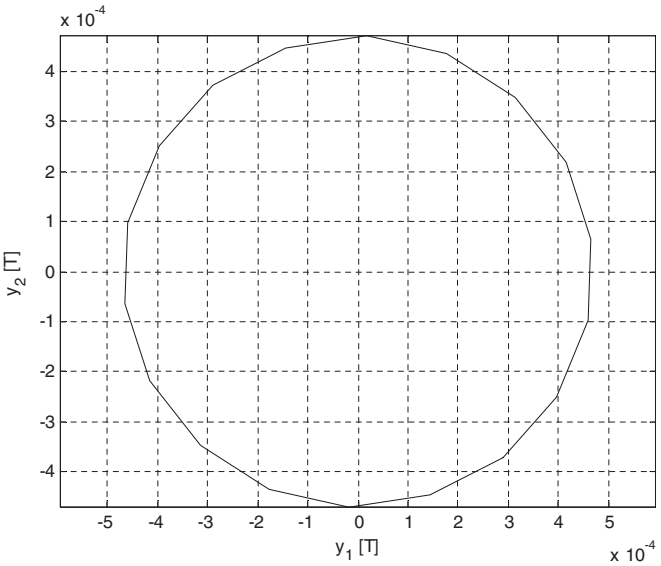

FIG. 15. The stabilizable region in terms of initial vertical magnetic field perturbations at the outboard midplane, following the BAP approach. y_1 and y_2 are at 90° phase to each other, corresponding to the cos and sin components of the $n=1$ sensor signal. The ELM control is assumed active. An ITER plasma is considered with $\beta_N=3.17$, for which the passive growth rate of the $n=1$ RWM is 30.0 s^{-1}.

diction. We point out that although in principle a 3D wall can remove spectrum degeneracy,[31] such that two distinguished eigenvalues appear with the same toroidal mode number, in the present case, the resulting difference between eigenvalues is smaller than the accuracy with which these eigenvalues are computed. For this reason, only one value is reported in Table I for each plasma pressure.

For the ITER wall geometry, the holes and the tubular extensions seem to be the two main 3D features that affect the passive stability of the RWM. More advanced computations with CARMA, by adding the blanket modules and the TF (toroidal field) coil cases, reduce the RWM growth rates by about 10% and 2%, respectively.[32] Inclusion of the OTS and bypasses also results in a minor modification of the mode growth rate.

TABLE I. Comparison of the passive growth rates (in s^{-1}) of the RWM for ITER plasmas, with a 2D vacuum-vessel (VV) model (column 4), a VV model including port holes (column 5) and including the tubular extensions, as shown in Fig. 14 (column 6). MARS-F computations always assume a complete axisymmetric wall (2D).

β_N	C_β	MARS-F	Coarse mesh2D VV	Coarse mesh VV+holes	Reference3D mesh
2.86	0.31	6.36	5.99	11.3	7.64
3.02	0.47	12.7	11.5	24.3	15.4
3.17	0.61	24.2	20.9	51.8	30.0
3.33	0.77	51.7	41.5	155	69.0
3.48	0.92	160.5	98.9	N.A.	272.0

C. Feedback results

Using the CARMA code, we pursue a control analysis for the RWM feedback stabilization in ITER. We follow two strategies. The first is called the best achievable performance (BAP) analysis.[24] The BAP principle can be approximately described in the following way. We seek the maximum level of initial plasma perturbations, for which a control voltage and a corresponding current signal can be found, that reduces the initial perturbation to zero in a finite time interval. Given voltage and current limits are applied to the above procedure. We use this strategy to investigate the "controllability" of the RWM in ITER at various β_N, taking into account the effect of 3D conducting wall structures. As for the active coils, we use the 3×9 in-vessel resonant magnetic perturbation (RMP) coils in ITER, designed primarily for the purpose of edge localized mode (ELM) mitigation. For the sensor signals, we use 18 pick-up coils equally spaced along the toroidal angle at the outboard midplane.

Figure 15 shows one example following the BAP strategy. We choose an ITER plasma with $\beta_N=3.17$, corresponding to $C_\beta=0.61$. A 3D double wall with holes and tubular extensions, as shown in Fig. 14, is assumed in the CARMA computation. The voltage and current limits are 28 V and 250 A, respectively, for all three sets of RMP coils (upper, middle, and lower). The last assumptions take into account that a large fraction of the control power is shared by the ELM control during the RWM feedback. The initial perturbation is defined by the vertical component of the magnetic field at the outboard midplane (poloidal field perturbation). Since nonaxisymmetric 3D conductors split the $n=1$ RWM into two modes, with the same n number but generally different growth rates,[31] the initial field perturbations are characterized by two signals, separated toroidally by 90° (for the

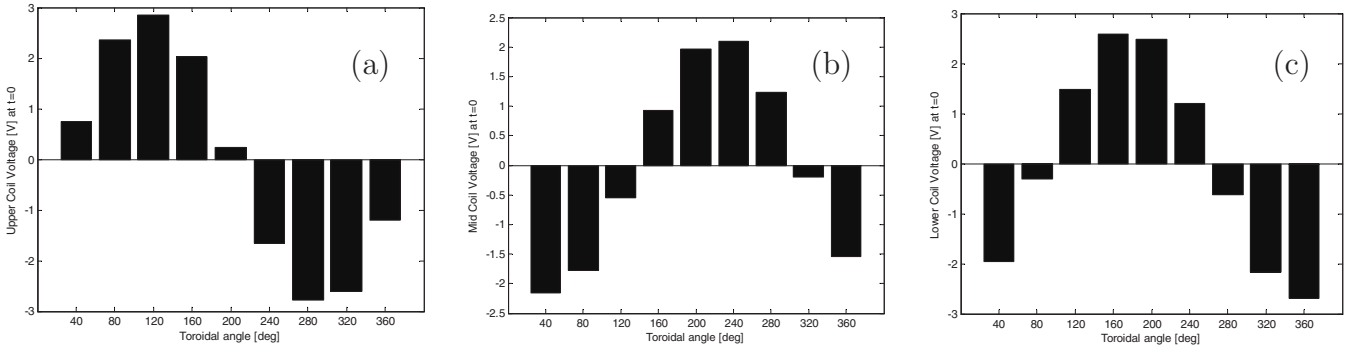

FIG. 16. The toroidal distribution of voltages in the ELM coils at $t=0$ for a perturbation at the border of the BAP region, as shown in Fig. 15. Shown are voltages for (a) upper coils, (b) middle coils, and (c) lower coils.

$n=1$ mode) and denoted by y_1 and y_2, respectively, in the figure. Within the boundary curve shown in Fig. 15, the RWM can be stabilized. The maximum field perturbation, that is still stabilizable within the voltage and current limits for the control coils, is about 4.6 G for this case.

For the same plasma and control configuration as above, Figs. 16(a)–16(c) show the voltage distribution along the toroidally spaced nine coils, for the upper, middle, and lower sets, respectively. The values are plotted for the moment when the feedback is switched on ($t=0$). An initial perturbation is chosen at the border of the BAP region shown in Fig. 15. The required voltages for the coils do not reach the limit. Instead, we find that the current limit is reached, as shown by Figs. 17(a)–17(c), for the coil current distribution at $t=0.0075$ s after the feedback is switched on.

The second strategy of the feedback study is to design an actual controller, which allows us to simulate the closed loop in the state-space variables. We search for a multivariable controller based on the LQG technique (linear quadratic regulator with Gaussian distributed noise).[39] Figure 18 shows one example of the control results, where we plot the simulated time trace of the closed loop for the coil current, using an optimal LQG controller found for the same plasma as in Fig. 15. Initial field perturbations are randomly generated within the amplitude of 4.6 G. The maximum coil current is within the limit of 250 A. The settling time is around 1 s.

We also performed a similar control study using the external error field correction coils (EFCC) designed for ITER. A comparable control performance (in terms of the maximum initial field perturbation) is achieved by assuming larger voltage and current limits for the coils, of 75 V and 20 kA, respectively. We point out that these results largely confirm the previous control analysis,[14] where a 2D wall geometry is assumed, and an optimal proportional-integral-derivative controller is designed for the same ITER plasmas using EFCC. The assumed voltage and current limits are higher in Ref. 14, which also allows a larger initial field perturbation reaching 15 G.

V. SUMMARY AND DISCUSSION

In this paper, we utilize a recently developed hybrid kinetic-MHD code MARS-K (Ref. 17) to study the RWM damping physics. Toroidal computations are performed for an equilibrium from DIII-D (discharge 125 701), where the critical ω_E rotation speed for RWM stability is measured to be about 0.3% of the Alfvén speed at the $q=2$ magnetic surface.[10] We compare the modeling results from both perturbative and self-consistent approaches, as well as with DIII-D experiments.

While the perturbative approach predicts a strong stabilization of the RWM, over a wide range of parameter space in C_β and ω_E, the self-consistent approach generally predicts less kinetic stabilization. In particular, the latter predicts the existence of new unstable branches of the RWM caused by kinetic resonances between the mode and the thermal particle precession drifts. An analytic model suggests that these unstable branches are primarily due to the nonlinearity of the

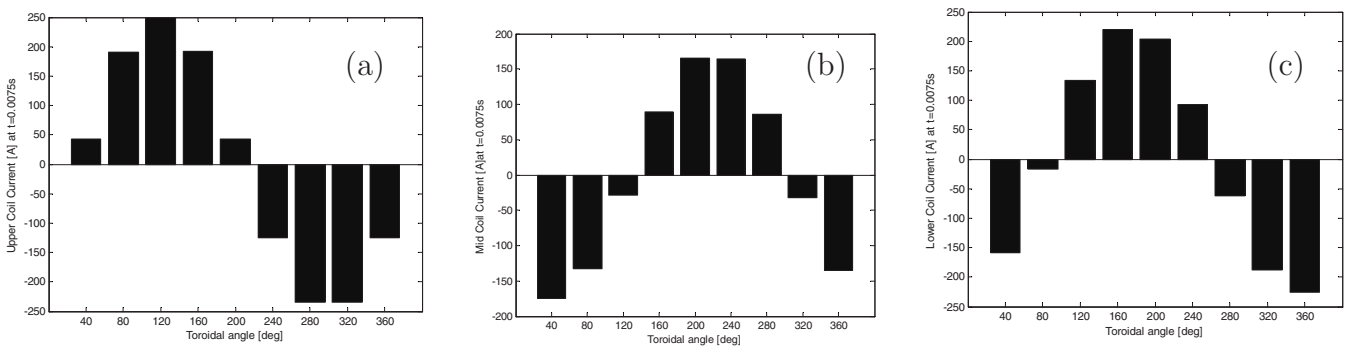

FIG. 17. The toroidal distribution of currents in the ELM coils at $t=0.0075$ s for the same perturbation at the border of the BAP region, as shown in Fig. 16. Shown are currents for (a) upper coils, (b) middle coils, and (c) lower coils.

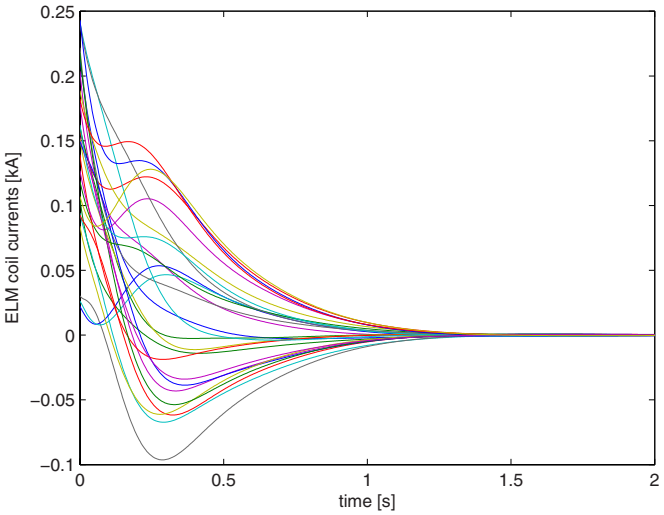

FIG. 18. (Color online) The RWM control simulations (the ELM coil currents) for an ITER equilibrium with β_N=3.17, assuming random initial field perturbation amplitude, and with a current limit of 250 A in all coils.

eigenvalue arising from the kinetic integrals in the self-consistent approach. No significant kinetic modification of the mode eigenfunction is observed in the self-consistent computations for these DIII-D plasmas, compared to that of the fluid RWM.

The self-consistent kinetic computations do *not* fully explain the DIII-D results. Additional damping physics may be required. In particular, the kinetic contribution from beam driven hot ions and from the thermal particle collision effect may change the conclusion. An adequate modeling of the hot ion effects may need to take into account the anisotropy of the particle distribution, as well as the finite radial excursion of hot ions crossing flux surfaces (finite banana width for trapped ions). This is part of our ongoing work. On the other hand, the unstable RWMs, excited due to the nonlinear coupling of the mode eigenvalue through the kinetic integrals, have common features with some of the unstable modes observed in the recent JT-60U experiments.[38]

An important aspect of the RWM stability and control prediction for ITER plasmas is to take into account the realistic 3D geometry of the conducting structures, including the vacuum vessels and coils. Extensive modeling work is carried out for ITER using the new 3D code CARMA.[23,24] The 3D features of ITER walls, such as the holes and the tubular extensions, have a significant influence on the eddy current flow, and hence on the passive stability of the mode. Detailed 3D modeling of RWM control using CARMA has established the maximum tolerable initial field perturbation level at given voltage and current limits for the in-vessel RMP coils in ITER. Assuming a coil current limit of 250 A, a multivariable, LQG-based optimal controller is realized, capable of stabilizing the RWM at β_N=3.17 for ITER, for an initial field perturbation amplitude within 4.6 G.

The present 3D modeling of the RWM control in ITER does not include the effects of plasma inertia, rotation and drift kinetic terms. A new version of CARMA, based on a new coupling scheme[28] between CARIDDI and MARS-K, will be developed and allow us to study all these combined effects.

ACKNOWLEDGMENTS

This work was partly funded by the Engineering and Physical Sciences Research Council (United Kingdom) and by the European Communities under the contract of Association between EURATOM and UKAEA. The views and opinions expressed herein do not necessarily reflect those of the European Commission. Work was partly conducted within the framework of the European Fusion Development Agreement. Work also supported by the U.S. Department of Energy under Grant No. DE-FG03-956ER54309.

[1] C. Kessel, J. Manickam, G. Rewoldt, and W. M. Tang, Phys. Rev. Lett. **72**, 1212 (1994).
[2] T. C. Hender, J. C. Wesley, J. Bialek, A. Bondeson, A. H. Boozer, R. J. Buttery, A. Garofalo, T. P. Goodman, R. S. Granetz, Y. Gribov, O. Gruber, M. Gryaznevich, G. Giruzzi, S. Guenter, N. Hayashi, P. Helander, C. C. Hegna, D. F. Howell, D. A. Humphreys, G. T. A. Huysmans, A. W. Hyatt, A. Isayama, S. C. Jardin, Y. Kawano, A. Kellman, C. Kessel, H. R. Koslowski, R. J. La Haye, E. Lazzaro, Y. Q. Liu, V. Lukash, J. Manickam, S. Medvedev, V. Mertens, S. V. Mirnov, Y. Nakamura, G. Navratil, M. Okabayashi, T. Ozeki, R. Paccagnella, G. Pautasso, F. Porcelli, V. D. Pustovitov, V. Riccardo, M. Sato, O. Sauter, M. J. Schaffer, M. Shimada, P. Sonato, E. J. Strait, M. Sugihara, M. Takechi, A. D. Turnbull, E. Westerhof, D. G. Whyte, R. Yoshino, H. Zohm, and the ITPA MHD, Disruption and Magnetic Control Topical Group, Nucl. Fusion **47**, S128 (2007).
[3] D. Gregoratto, A. Bondeson, M. S. Chu, and A. M. Garofalo, Plasma Phys. Controlled Fusion **43**, 1425 (2001).
[4] L.-J. Zheng, M. Kotschenreuther, and M. S. Chu, Phys. Rev. Lett. **95**, 255003 (2005).
[5] A. Bondeson and D. J. Ward, Phys. Rev. Lett. **72**, 2709 (1994).
[6] R. Betti, Phys. Rev. Lett. **74**, 2949 (1995).
[7] J. Finn, Phys. Plasmas **2**, 198 (1995).
[8] C. G. Gimblett and R. J. Hastie, Phys. Plasmas **7**, 258 (2000).
[9] R. Fitzpatrick and A. Y. Aydemir, Nucl. Fusion **36**, 11 (1996).
[10] H. Reimerdes, A. M. Garofalo, G. L. Jackson, M. Okabayashi, E. J. Strait, M. S. Chu, Y. In, R. J. La Haye, M. J. Lanctot, Y. Q. Liu, G. A. Navratil, W. M. Solomon, H. Takahashi, and R. J. Groebner, Phys. Rev. Lett. **98**, 055001 (2007).
[11] E. J. Strait, A. M. Garofalo, G. L. Jackson, M. Okabayashi, H. Reimerdes, M. S. Chu, R. Fitzpatrick, R. J. Groebner, Y. In, R. J. LaHaye, M. J. Lanctot, Y. Q. Liu, G. A. Navratil, W. M. Solomon, and H. Takahashi, and the DIII-D Team, Phys. Plasmas **14**, 056101 (2007).
[12] M. Takechi, G. Matsunaga, N. Aiba, T. Fujita, T. Ozeki, Y. Koide, Y. Sakamoto, G. Kurita, A. Isayama, Y. Kamada, and the JT-60 Team, Phys. Rev. Lett. **98**, 055002 (2007).
[13] A. Bondeson and M. S. Chu, Phys. Plasmas **3**, 3013 (1996).
[14] Y. Q. Liu, A. Bondeson, Y. Gribov, and A. Polevoi, Nucl. Fusion **44**, 232 (2004).
[15] B. Hu and R. Betti, Phys. Rev. Lett. **93**, 105002 (2004).
[16] R. Aymar, P. Barabaschi, and Y. Shimomura, Plasma Phys. Controlled Fusion **44**, 519 (2002).
[17] Y. Q. Liu, M. S. Chu, I. T. Chapman, and T. C. Hender, Phys. Plasmas **15**, 112503 (2008).
[18] T. M. Antonsen and Y. C. Lee, Phys. Fluids **25**, 132 (1982).
[19] F. Porcelli, R. Stankiewicz, W. Kerner, and H. L. Berk, Phys. Plasmas **1**, 470 (1994).
[20] S. D. Pinches, L. C. Appel, J. Candy, S. E. Sharapov, H. L. Berk, D. Borba, B. N. Breizman, T. C. Hender, K. I. Hopcraft, G. T. A. Huysmans, and W. Kerner, Comput. Phys. Commun. **111**, 133 (1998).
[21] I. T. Chapman, M. P. Gryaznevich, C. G. Gimblett, T. C. Hender, D. F. Howell, Y. Q. Liu, S. D. Pinches, and JETEFDA Contributors, Plasma Phys. Controlled Fusion **51**, 055015 (2009).
[22] Y. Q. Liu, M. S. Chu, I. T. Chapman, and T. C. Hender, Nucl. Fusion **49**, 035004 (2009).
[23] R. Albanese, Y. Q. Liu, A. Portone, G. Rubinacci, and F. Villone, IEEE Trans. Magn. **44**, 1654 (2008).
[24] A. Portone, F. Villone, Y. Q. Liu, R. Albanese, and G. Rubinacci, Plasma Phys. Controlled Fusion **50**, 085004 (2008).

[25]Y. Q. Liu, A. Bondeson, C. M. Fransson, B. Lennartson, and C. Breitholtz, Phys. Plasmas **7**, 3681 (2000).
[26]R. Albanese and G. Rubinacci, Adv. Imaging Electron Phys. **102**, 1 (1998).
[27]V. D. Pustovitov, Plasma Phys. Controlled Fusion **50**, 105001 (2008).
[28]Y. Q. Liu, R. A. Albanese, A. Portone, G. Rubinacci, and F. Villone, Phys. Plasmas **15**, 072516 (2008).
[29]J. Bialek, A. H. Boozer, M. E. Mauel, and G. A. Navratil, Phys. Plasmas **8**, 2170 (2001).
[30]P. Merkel and M. Sempf, *21st IAEA Fusion Energy Conference*, 2006, Chengdu, China (International Atomic Energy Agency, Vienna, 2006), Paper No. TH/P3-8.
[31]F. Villone, Y. Q. Liu, R. Paccagnella, G. Rubinacci, and T. Bolzonella, Phys. Rev. Lett. **100**, 255005 (2008).
[32]G. Rubinacci, S. Ventre, F. Villone, and Y. Liu, J. Comput. Physics **228**, 1562 (2009).
[33]H. Reimerdes, A. M. Garofalo, M. Okabayashi, E. J. Strait, R. Betti, M. S. Chu, B. Hu, Y. In, G. L. Jackson, R. J. La Haye, M. J. Lanctot, Y. Q. Liu, G. A. Navratil, W. M. Solomon, H. Takahashi, R. J. Groebner, and the DIII-D Team, Plasma Phys. Controlled Fusion **49**, B349 (2007).
[34]E. J. Strait and DIII/D Team, *22nd IAEA Fusion Energy Conference*, 2008, Geneva, Switzerland (International Atomic Energy Agency, Vienna, 2006), Paper No. OV/1-4.
[35]S. W. Haney and J. P. Freidberg, Phys. Fluids B **1**, 1637 (1989).
[36]M. S. Chu, J. M. Greene, T. H. Jensen, R. L. Miller, A. Bondeson, R. W. Johnson, and M. E. Mauel, Phys. Plasmas **2**, 2236 (1995).
[37]Y. Q. Liu, M. S. Chu, C. G. Gimblett, and R. J. Hastie, Phys. Plasmas **15**, 092505 (2008).
[38]G. Matsunaga, Y. Sakamoto, N. Aiba, K. Shinohara, M. Takechi, T. Suzuki, T. Fujita, A. Isayama, N. Oyama, N. Asakura, Y. Kamada, T. Ozeki, and the JT-60 Team, *22nd IAEA Fusion Energy Conference*, 2008, Geneva, Switzerland (International Atomic Energy Agency, Vienna, 2006), Paper No. EX/5–2.
[39]F. L. Lewis and V. L. Syrmos, *Optimal Control* (Wiley-IEEE, New York, 1995), p. 478.